

Article

# Dry Reforming of Methane Using Ce-modified Ni Supported on 8%PO<sub>4</sub> + ZrO<sub>2</sub> Catalysts

Ahmed A. Ibrahim, Ahmed S. Al-Fatesh \*, Nadavala Siva Kumar, Ahmed E. Abasaheed,  
Samsudeen O. Kasim and Anis H. Fakeeha

Chemical Engineering Department, College of Engineering, King Saud University, P.O. Box 800, Riyadh 11421, Saudi Arabia; aididwthts2011@gmail.com (A.A.I.); snadavala@ksu.edu.sa (N.S.K.); abasaheed@ksu.edu.sa (A.E.A.); sofkolajide2@gmail.com (S.O.K.); anishf@ksu.edu.sa (A.H.F.)

\* Correspondence: aalfatesh@ksu.edu.sa; Tel.: +966-11-467-6859; Fax: +966114678770

Received: 24 December 2019; Accepted: 28 January 2020; Published: 18 February 2020



**Abstract:** Dry reforming of methane (DRM) was studied in the light of Ni supported on 8%PO<sub>4</sub> + ZrO<sub>2</sub> catalysts. Cerium was used to modify the Ni active metal. Different percentage loadings of Ce (1%, 1.5%, 2%, 2.5%, 3%, and 5%) were tested. The wet incipient impregnation method was used for the preparation of all catalysts. The catalysts were activated at 700 °C for ½ h. The reactions were performed at 800 °C using a gas hourly space velocity of 28,000 mL (h·gcat)<sup>-1</sup>. X-ray diffraction (XRD), N<sub>2</sub> physisorption, hydrogen temperature programmed reduction (H<sub>2</sub>-TPR), temperature programmed oxidation (TPO), temperature programmed desorption (TPD), and thermogravimetric analysis (TGA) were used for characterizing the catalysts. The TGA analysis depicted minor amounts of carbon deposition. The CO<sub>2</sub>-TPD results showed that Ce enhanced the basicity of the catalysts. The 3% Ce loading possessed the highest surface area, the largest pore volume, and the greatest pore diameter. All the promoted catalysts enhanced the conversions of CH<sub>4</sub> and CO<sub>2</sub>. Among the promoted catalysts tested, the 10Ni + 3%Ce/8%PO<sub>4</sub> + ZrO<sub>2</sub> catalyst system operated at 1 bar and at 800 °C gave the highest conversions of CH<sub>4</sub> (95%) and CO<sub>2</sub> (96%). The stability profile of Cerium-modified catalysts (10%Ni/8%PO<sub>4</sub> + ZrO<sub>2</sub>) depicted steady CH<sub>4</sub> and CO<sub>2</sub> conversions during the 7.5 h time on stream.

**Keywords:** cerium; dry reforming of methane; PO<sub>4</sub>; supported nickel; ZrO<sub>2</sub>

## 1. Introduction

Dry reforming of methane (DRM) uses a favorable reaction that transforms two greenhouse gases, methane and carbon dioxide, into a synthesis gas, which is a beneficial product [1–5]. Moreover, DRM can be a potential process for the improvement of biogas composed largely by CO<sub>2</sub> and CH<sub>4</sub> [6,7]. The utilization of fossil fuels generates greenhouse gases, which contribute significantly to climate change and cause global warming [8–10]. The methane gas constitutes more than 80% of natural gas, and therefore, its conversion plays a vital role in the future energy supply, since it produces energy carriers such as carbonyl and dimethyl ether. The produced synthesis gas is composed of H<sub>2</sub> and CO, which are versatile intermediates for many useful chemical products such as liquid fuels obtained via Fischer–Tropsch synthesis, light olefins, and hydrocarbons [9,11,12]. DRM can also be employed as chemical storage for renewable energy on account of its highly endothermic nature [13]. Consequently, broad studies are focused on developing a dry reforming process for syngas production. The absence of a catalyst that is stable under the reaction conditions hinders the commercialization of the dry reforming of methane process. For this reason, the utilization of an effective catalyst is essential. For instance, the use of noble metals such as Pt, Rh, Pd, Ru, and Ir distributed on support are competently used for dry reforming of CH<sub>4</sub> [14–16]. Arandiyani et al. [17] investigated the effect of noble metals on

the dry reforming of  $\text{CH}_4$ . They tested the catalytic activity over  $\text{La}_{0.4}\text{M}_{0.6}\text{Al}_{0.2}\text{Ni}_{0.8}\text{O}_3$  ( $\text{M} = \text{Pt}, \text{Pd}, \text{Ru}, \text{Rh}, \text{Ir}$ ) perovskite-type oxides with a surface area of  $3.26\text{--}4.14 \text{ m}^2/\text{g}$ . It was obtained that the  $\text{La}_{0.4}\text{Rh}_{0.6}\text{Al}_{0.2}\text{Ni}_{0.8}\text{O}_3$  catalyst revealed the best catalytic performance due to its high surface area, surface oxygen concentration, and good low-temperature reducibility. El Hassan et al. [18] studied the influence of Rh (0.2 and 0.5 wt %) to the Co/SBA-15 catalyst in the catalytic performance of dry reforming of  $\text{CH}_4$ . It was found that Rh favored Co stabilization in the mesopores and was reduced at a much lower temperature. The nature of coke was affected and less  $\gamma$ -carbon formed on the Rh-containing sample. However, because of the high prices and limited availability of noble metals, the research has also focused on transition metals such as Co, Ni, Ti, which are broadly used for this process because of their high activity [19]. However, these catalysts are prone to quick deactivation due to coke deposition. Within the catalysts, Ni depicted the greatest performance due to its strong ability to break C–C/C–H bonds and activate  $\text{CH}_4$  [20]. AKri et al. [21] elaborated the dry reforming of  $\text{CH}_4$  employing atomically dispersed Ni atoms, stabilized by interaction with Ce-doped hydroxyapatite. Their results evidenced that the catalyst was very active and that isolated Ni atoms were inherently coke resistant. Ce doping of hydroxyapatite brought strong metal–support interactions which stabilized Ni single atoms toward sintering and favored the selective activation of only the first C–H bond in  $\text{CH}_4$ . Goula et al. [22] investigated nickel supported on Zr modified with  $\text{CeO}_2$  or  $\text{La}_2\text{O}_3$  catalysts for the dry reforming of a  $\text{CH}_4$  reaction. Although bare Zr support provided adequate activity and stability, however, the modified Zr support with Ce and La enhanced basicity and oxygen ion lability values and therefore gave better activity and stability performance. Abba et al. [23] used natural phosphate support for Ni in the reforming reaction of methane. They found that the support modification by means of an acid gave a very active and stable Ni-based catalyst. Ibrahim et al. [24] studied the dry reforming of  $\text{CH}_4$  using phosphate zirconia supported nickel catalysts ( $x\% \text{Ni}/8\% \text{PO}_4\text{-Zr}$ , where  $x = 5, 10, 15$  or  $20$ ). The result exhibited that activity and stability was intensely related to nickel loading, whereas the highest performance was recorded for a catalyst having a Ni loading of 10 wt %. Al-Fatesh et al. [5] investigated the dry reforming of  $\text{CH}_4$  over combined Mg and Ce on Ni-based catalysts supported on  $\gamma\text{-Al}_2\text{O}_3$  support doped with 3.0 wt. %  $\text{TiO}_2$ . Cerium and magnesium oxides strengthened the interaction between the nickel and the support, and hence the catalytic activity was substantially improved. Then again, Fatish et al. [4] reported the effect whereby Ce promoted Ni supported on lanthanum-modified zirconium oxides in the dry reforming of  $\text{CH}_4$ . The result established that the reduction properties of the catalysts were considerably improved upon  $\text{La}_2\text{O}_3$  modification. The lanthanum incorporated into the zirconium support and the t- $\text{ZrO}_2$  phase was secure and highly stabilized, leading to greater catalytic performance. Remarkably,  $\text{CH}_4$  conversion increased twice, and  $\text{CO}_2$  conversion increased to 1.5 times that of pristine Ni/ $\text{ZrO}_2$ . Deactivation arising from the coke deposition is the chief obstacle in the use of Ni-containing catalyst [25]; however, it can be overcome by the addition of promoters. Promoting elements play substantial roles in improving the catalyst, even though they are used in slight quantities [26]. The role of dopants on the catalytic activity for  $\text{CO}_2$  reforming of  $\text{CH}_4$  was examined on  $\text{Ni}/\text{Me}_{0.15}\text{Ce}_{0.85}\text{O}_{2-\delta}$  with  $\text{Me} = \text{Zr}^{4+}, \text{La}^{3+}$  or  $\text{Sm}^{3+}$  catalysts [27]. Zr-doped catalyst gave the highest activity, while Sm and La-doped catalysts produced the lowest coke formation. The type of dopants affected the Ni–support interaction and the electronic state of the metal catalyst. Veen and Li modified the performance of Ni-catalyzed dry reforming of  $\text{CH}_4$  and carbon deposition by the use of Ni– $\text{CeO}_{2-x}$  interaction [28]. The result of the  $\text{H}_2$  reduction beyond  $500 \text{ }^\circ\text{C}$  created a strong bonding between Ni and  $\text{CeO}_2$  that prevented Ni particle sintering. A reduction temperature of  $600 \text{ }^\circ\text{C}$  and above brought the decoration/encapsulation of Ni nanoparticles by a thin layer of reduced  $\text{CeO}_2$  support with partial coverage of the Ni surface.

Kalai et al. investigated an Ni-based catalyst promoted with Ce in biogas reforming, and their results displayed that an active catalyst resistant to sintering and coke deposition was formed by a higher Ce/Ni ratio [29]. The promotional influence of various kinds of metal supported over Ni/SBA-15 was investigated via the dry reforming of  $\text{CH}_4$  [30]. It was found that the metal promoters could successfully improve Ni dispersion over the SBA-15's siliceous framework and control the NiO

crystallize sizes. Generally, the performance of a catalyst is determined not only by the active species but also by the type of support. Therefore, another method of reducing the coke generation is the employment of proper supports, which decreases sintering and carbon formation [31]. The supports are vital in improving activity and decreasing carbon production during the dry methane-reforming process. Basic supports help in the gasification of the carbon species and consequently control the carbon deposition. Moreover, their existence circumvents the destruction of the active phases by sintering [32].

Lino et al. investigated methane's tri-reforming reaction performance using nickel catalysts supported on magnesium aluminate promoted with  $ZrO_2$ ,  $CeZrO_2$ , and  $CeO_2$  [33]. Their results exhibited less coke formation and growth conversions when Zr and Ce-Zr promoted catalysts were used. Zirconia is used in many chemical reactions as a promoter and support because of its great thermal stability, medium basicity and acidity, and oxygen mobility [34]. The investigation of Li et al. found that adding  $ZrO_2$  in  $Ni/Al_2O_3$  had a superb catalytic output owing to the evenly spread minor metallic nickel particles, which helped the reducibility of the nickel oxides and the metal-support interaction [35]. On the other hand, Li and co-authors reported the influence of  $PO_4$  upon the activity in perchlorate and stated enough endurance of Fe catalyst having a composition up to 5.0 M  $H_3PO_4$  [36]. The anions of phosphate displayed an insignificant result in reducing the activity.

The aim of this work is to analyze the activity, stability, and efficiency of 10% Ni-containing catalyst prepared via the impregnation technique and operated at 1 bar and at 800 °C in DRM. An Ni catalyst is promoted with different loading of Ce (1%–5%) and supported upon 8%  $PO_4$ - $ZrO_2$ .

## 2. Results and Discussion

### 2.1. Catalyst Characterization

Figure 1A depicts the  $N_2$  adsorption/desorption isotherms for the non-promoted and promoted catalysts, calcined at 600 °C. The  $N_2$  adsorption/desorption isotherms fall under the type-IV classification. In accordance with the International Union of Pure and Applied Chemistry (IUPAC) classification, mesoporous materials display the observed isotherm profiles. The first region of the isotherm can be ascribed to the adsorption of the monolayer-multilayer. The existence of mesoporous forms the hysteresis after an approximate  $P/P_0 = 0.4$ . Additionally, at the high  $P/P_0$ , from 0.4 to 1.0, the H3 type of hysteresis loop is detected, which verifies the mesoporosity of the catalysts. Meanwhile, Figure 1B compares the distributions of pore size obtained by the Barrett, Joyner, and Halenda (BJH) method. It is evident that the distributions of pore size are narrow, showing that there existed only one type of pore, confirming the mesoporosity, as the pore diameter lies between 2 and 50 nm. Table 1 depicts the textural properties, which include the surface area, pore size, and pore diameters of 10% Ni catalysts supported by 8% $PO_4$  and  $ZrO_2$  and promoted by different amounts of Ce.

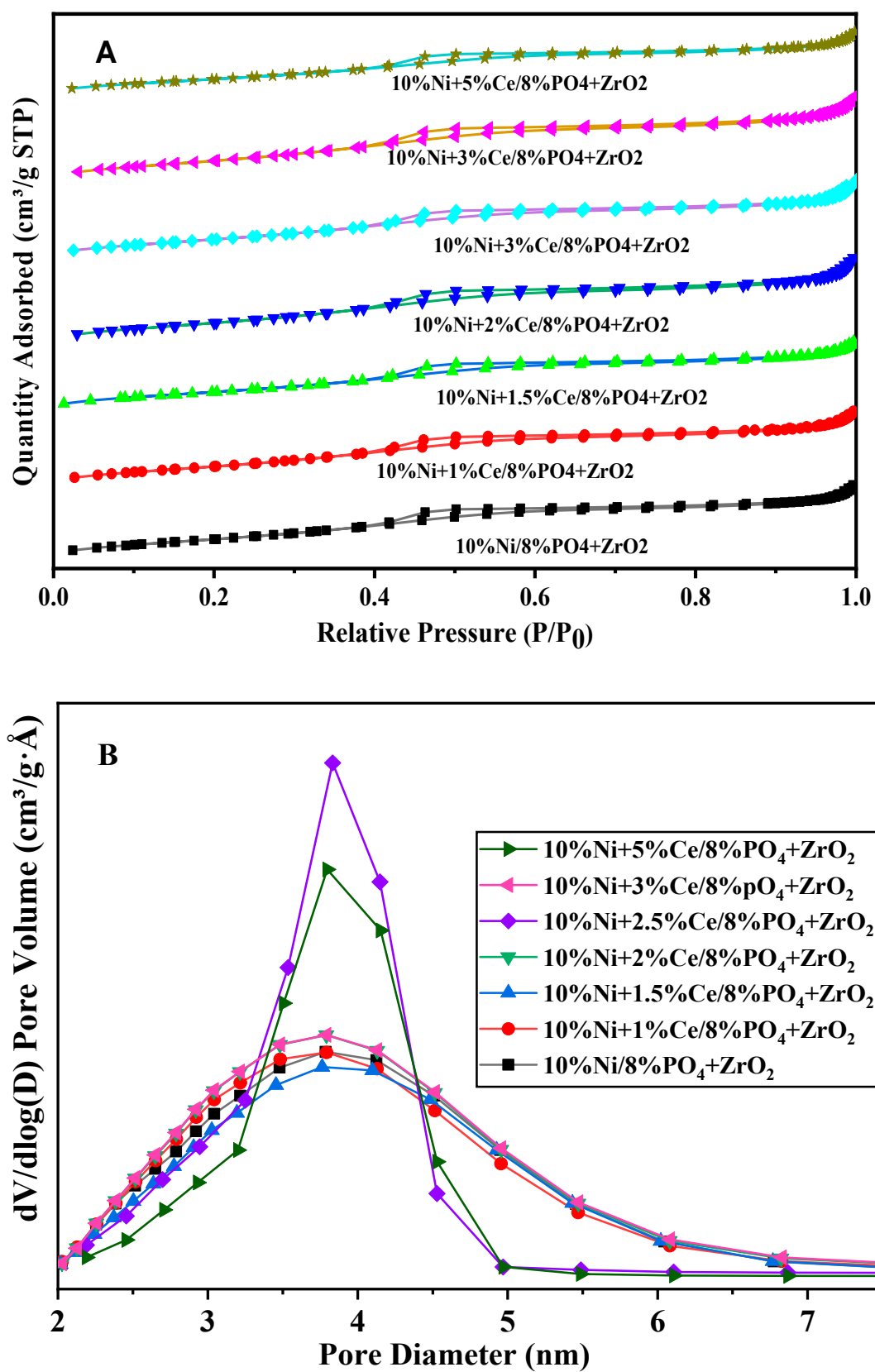


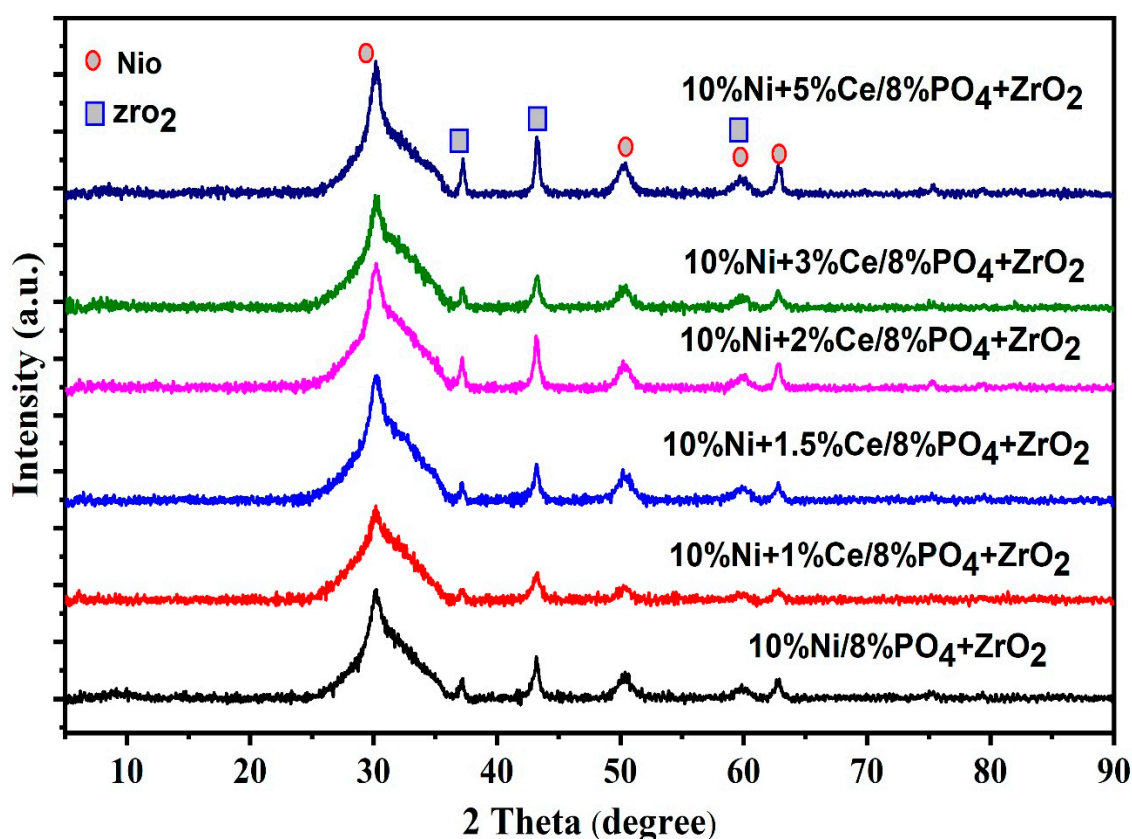
Figure 1. Nitrogen adsorption–desorption isotherms (A) and pore size distribution (B) diameter of fresh catalysts calcined at 600 °C.

**Table 1.** Textural properties of 10% Ni catalysts supported by 8%PO<sub>4</sub> and ZrO<sub>2</sub> and promoted by different amounts of cerium.

Catalyst	BET <sup>1</sup> Surface Area (m <sup>2</sup> /g)	Av. Pore Diameter (nm)	Pore Volume (cm <sup>3</sup> /g)
10%NiO/8%PO <sub>4</sub> + ZrO <sub>2</sub>	157.5	0.2	4.45
10%NiO + 1%Ce/8%PO <sub>4</sub> + ZrO <sub>2</sub>	157.5	0.2	4.45
10%NiO + 1.5%Ce/8%PO <sub>4</sub> + ZrO <sub>2</sub>	145.2	0.18	4.46
10%NiO + 2%Ce/8%PO <sub>4</sub> + ZrO <sub>2</sub>	166.7	0.22	4.67
10%NiO + 2.5%Ce/8%PO <sub>4</sub> + ZrO <sub>2</sub>	155.0	0.20	4.60
10%NiO + 3%Ce/8%PO <sub>4</sub> + ZrO <sub>2</sub>	168.2	0.22	4.67
10%NiO + 5%Ce/8%PO <sub>4</sub> + ZrO <sub>2</sub>	127.2	0.16	4.55

<sup>1</sup> BET- Brunauer-Emmett-Teller.

XRD patterns of 10Ni+X%Ce/8%PO<sub>4</sub>+ZrO<sub>2</sub> catalysts (X = 0, 1, 1.5, 2, 3, 5) are shown in Figure 2. The result indicated that the quantity of the promoter did not significantly influence the interaction between NiO and the support. The cubic phase of NiO is present in XRD patterns. The diffraction peaks at 2θ = 38.2, 43.8, and 61.5 were ascribed to NiO (JCPDS #47-1049), while the peaks at 2θ = 30.2 matched the monoclinic phase of ZrO<sub>2</sub>, and 38.2, 51.8, and 61.5 matched the tetragonal phase of ZrO<sub>2</sub> (JCPDS #50-1089).

**Figure 2.** X-ray diffraction patterns of 10Ni + x%Ce/8%PO<sub>4</sub> + ZrO<sub>2</sub> catalysts (x = 0, 1, 1.5, 2, 3, 5) calcined at 600 °C.

The H<sub>2</sub>-TPR profiles of 10Ni/8%PO<sub>4</sub> + ZrO<sub>2</sub>, 10Ni + 1%Ce/8%PO<sub>4</sub> + ZrO<sub>2</sub>, 10Ni + 2%Ce/8%PO<sub>4</sub> + ZrO<sub>2</sub>, 10Ni + 3%Ce/8%PO<sub>4</sub> + ZrO<sub>2</sub>, and 10Ni + 5%Ce/8%PO<sub>4</sub> + ZrO<sub>2</sub> are presented in Figure 3.

In all catalysts, wide reduction peaks related to the reduction of NiO were detected, but the mode of reduction of the catalysts was somewhat different. Peak maxima at 300–334, 564–593, and 732–780 °C were observed. The peak in the low temperature was ascribed to the non-associated NiO species, while the other peaks that appeared at the greater temperature were attributed to the NiO<sub>x</sub> complex species, where the support–metal interactions were high [37]. According to earlier literature, the reduction of catalysts at 300–334 °C was attributed to the free NiO species that had insufficient interaction with the support [38]. Alternatively, the peaks of catalyst at 588–593 and 732–780 °C were credited to the moderately strong and non-weakly interacting NiO species [39]. In general, there is no significant difference in the reduction temperature of the promoted and unpromoted catalysts. Table 2 illustrated the TPR results studied for the catalyst samples, in respect of amount of H<sub>2</sub> uptake, temperature of peak maxima (T<sub>M</sub>), and percentage reduction degree. The 10%Ni + 3%Ce/8%PO<sub>4</sub> + ZrO<sub>2</sub> catalyst gave the highest value.

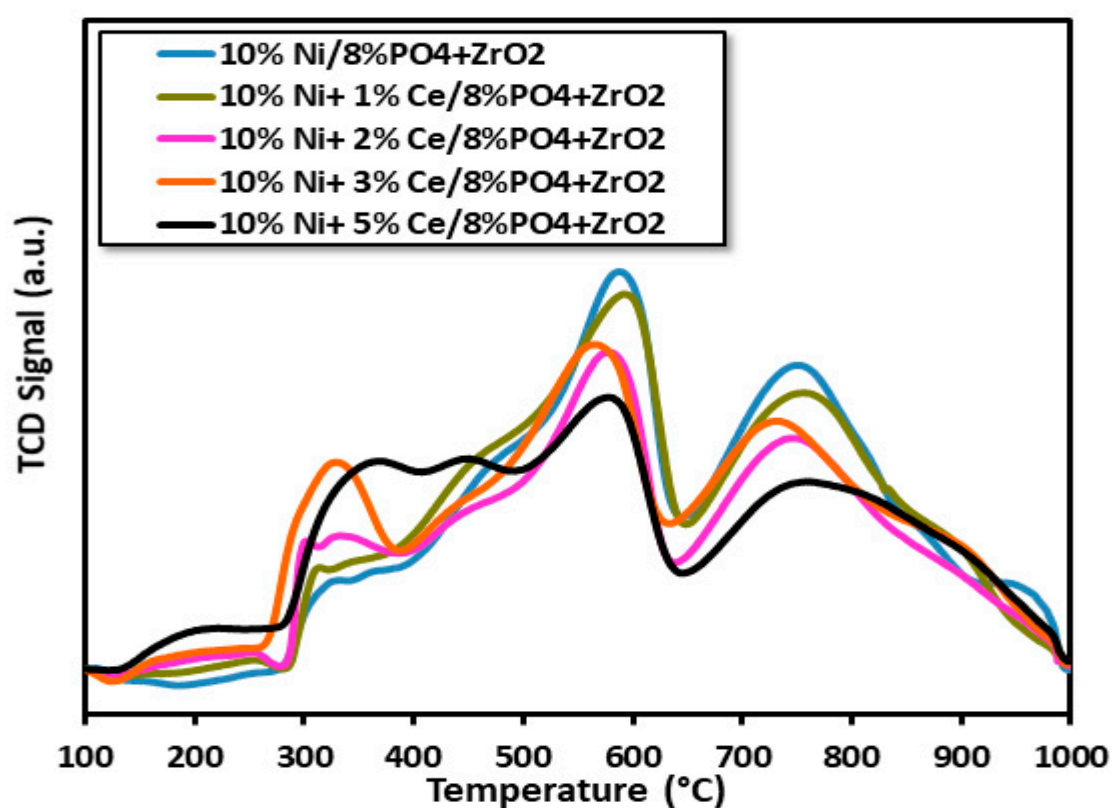


Figure 3. TPR-H<sub>2</sub> profiles of the reduced catalysts calcined at 600 °C.

Table 2. TPR data of the studied catalyst samples in terms of amount of H<sub>2</sub> consumption and temperature of peak maxima (T<sub>M</sub>).

Catalysts	H <sub>2</sub> Uptake (mmole/g)	T <sub>M1</sub> (°C)	T <sub>M2</sub> (°C)	T <sub>M3</sub> (°C)	Reduction Degree (%)
10%Ni/8%PO <sub>4</sub> + ZrO <sub>2</sub>	3.176	-	588	750	1.86
10%Ni + 1%Ce/8%PO <sub>4</sub> + ZrO <sub>2</sub>	3.023	-	593	780	1.77
10%Ni + 2%Ce/8%PO <sub>4</sub> + ZrO <sub>2</sub>	2.956	300	578	746	1.73
10%Ni + 3%Ce/8%PO <sub>4</sub> + ZrO <sub>2</sub>	2.517	329	564	732	2.44
10%Ni + 5%Ce/8%PO <sub>4</sub> + ZrO <sub>2</sub>	2.796	334	577	755	1.64

The CO<sub>2</sub>-TPD profile of 10Ni + x%Ce/8% PO<sub>4</sub>-ZrO<sub>2</sub> (x = 0, 1, 3, and 5) catalyst samples are exhibited in Figure 4. The CO<sub>2</sub>-TPD profile represents the level of interaction of CO<sub>2</sub> with the catalyst surface as well as the basic profile of the catalyst surface. In the low-temperature range (50–200 °C),

CO<sub>2</sub> reacts with the basic hydroxyl species on the surface, while at the medium temperature range (200–450 °C), it reacts with basic surface oxygen anion; lastly, it interacts with the lattice oxygen anions at the high-temperature range (450–800 °C) [40,41]. Commonly, CO<sub>2</sub> adsorption capacity and dissociation are improved, raising the basicity of the catalyst. In turn, this reduces carbon deposition over the surface and hence lowers the catalyst deactivation [42,43]. Four principal adsorption peaks could be recognized with maxima at around 90 °C, 170 °C, 250 °C, and 640 °C, respectively for Ce-promoted catalysts. Meanwhile, the unpromoted catalyst gives three adsorption peaks and does not generate peaks beyond 250 °C. The peaks could be allocated to non-strong, Brønsted basic sites, adequate strength basic ‘Lewis acid-base sites’, and strong basic sites ‘Lewis basic sites’. Thus, the addition of the cerium enhanced the basicity. Table 3 displays the basicity strength of various catalysts. It is obvious that 3% of Ce gave the highest amount of total basicity.

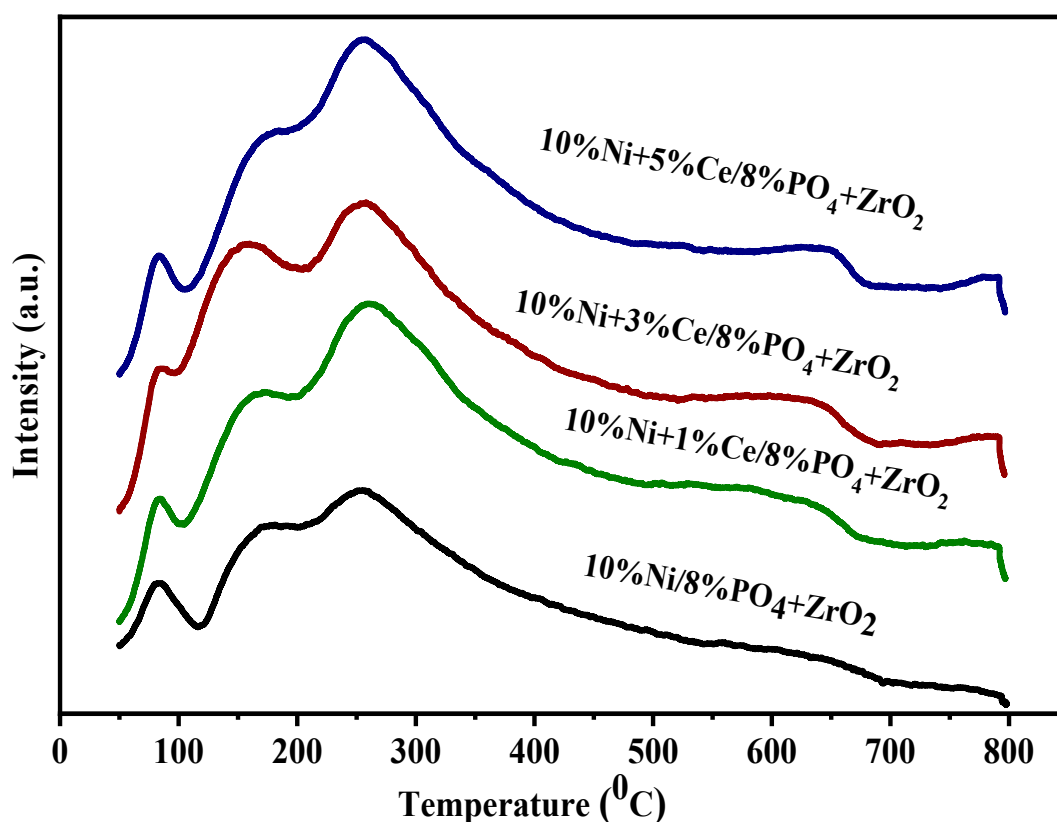


Figure 4. CO<sub>2</sub>-TPD profiles of 10Ni+z%Ce/8% PO<sub>4</sub>-ZrO<sub>2</sub> (z = 0, 1, 3, and 5) catalysts.

Table 3. Distribution of basic sites for Ni-supported catalysts.

Sample	Weak Basic Sites (μmol/g)	Medium Basic Sites (μmol/g)	Strong Basic Sites (μmol/g)	Total Basicity (μmol/g)
10Ni/8%PO <sub>4</sub> + ZrO <sub>2</sub>	18.027	19.957	-	37.984
10Ni + 2%Ce/8%PO <sub>4</sub> + ZrO <sub>2</sub>	18.019	40.213	-	58.232
10Ni + 3%Ce/8%PO <sub>4</sub> + ZrO <sub>2</sub>	30.881	47.051	-	77.932
10Ni + 5%Ce/8%PO <sub>4</sub> + ZrO <sub>2</sub>	24.456	24.353	-	48.809

## 2.2. Catalyst Activity

The experimental results of the reactor operated at the desired experimental conditions at 800 °C with support and in the absence of the active metals displayed the lack of activity. Figure 5A showed the CH<sub>4</sub> conversion and stability for a reaction period of 7.5 h for the catalysts calcined at 600 °C. The activity of the non-promoted catalysts started at 77% and reduced and stabilized to about 72%. Virtually all the promoted catalysts exhibited similar patterns. The addition of the promoter enhanced

the conversion from 15% to 24%. The catalyst promoted with 3% Ce generated the highest conversion and hence the best improvement. When the promoter loading was increased to 5%, the conversion was reduced.

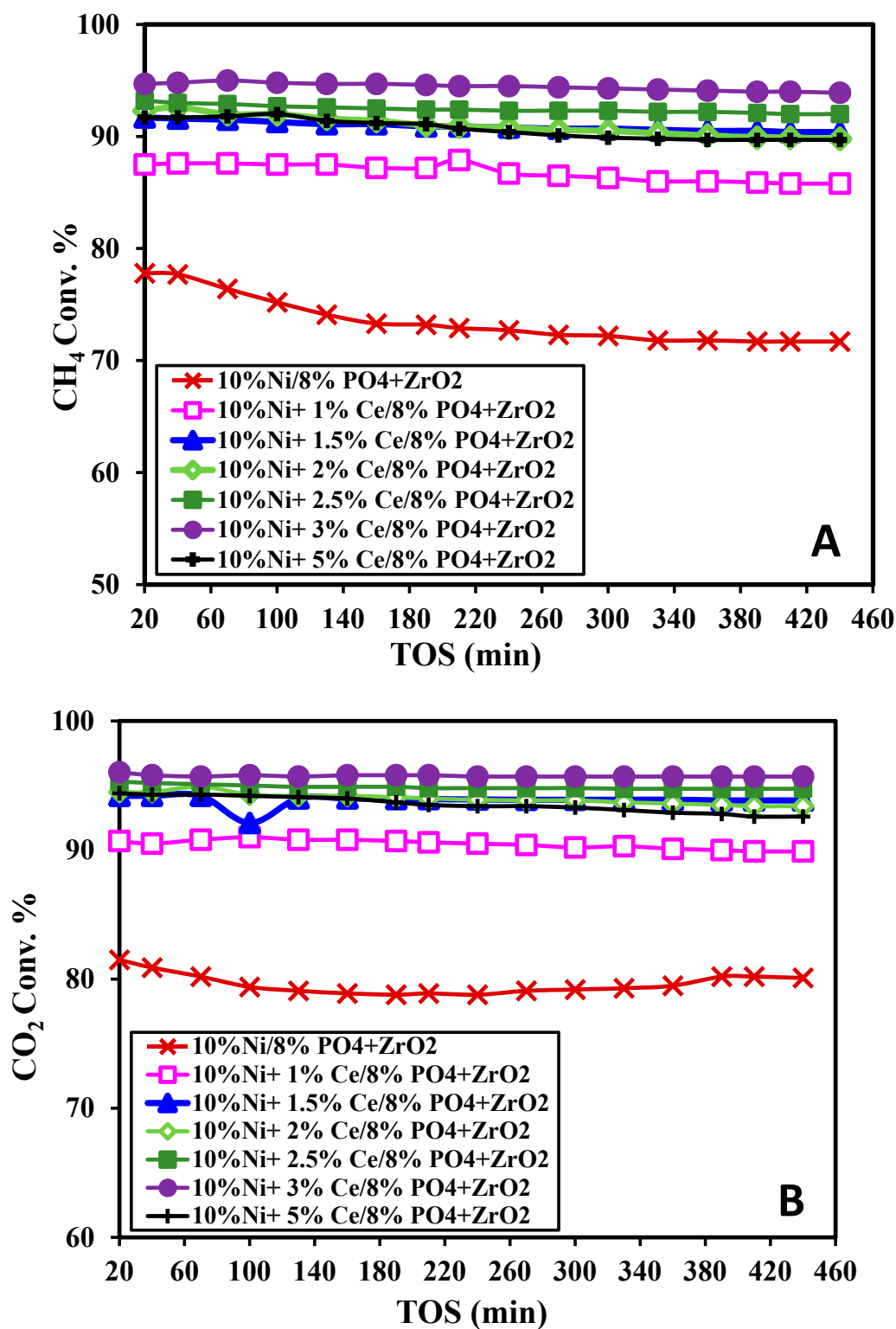


**Figure 5.** Catalytic activity of 10Ni + x% Ce/8% PO<sub>4</sub> + ZrO<sub>2</sub> (x = 0, 1, 1.5, 2, 2.5, 3.5, and 5) catalyst calcined at 600 °C, operated at 800 °C, GHSV = 28000 (mL/g/h) (A) CH<sub>4</sub> conversion against time-on-stream (TOS) (B) CO<sub>2</sub> conversion against TOS.

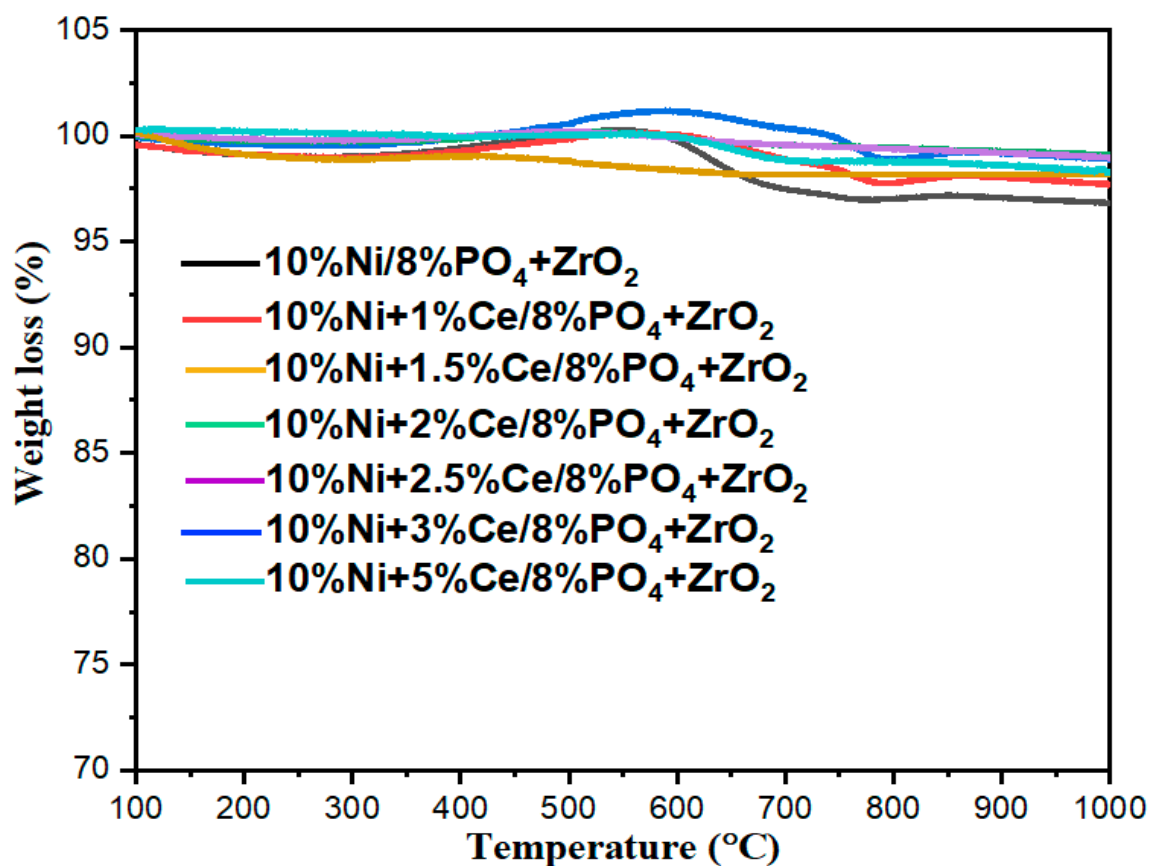
Figure 5B illustrated the results of CO<sub>2</sub> conversion versus time on stream, using the catalysts calcined at 600 °C and activated at 700 °C. The CO<sub>2</sub> conversions were greater than the corresponding CH<sub>4</sub> conversion. This was because the H<sub>2</sub> was produced from the reforming participates in a side reaction by initiating a parallel reverse water gas shift reaction (RWGS) (CO<sub>2</sub> + H<sub>2</sub> → CO + H<sub>2</sub>O) [44]. The Figure 5B profile was similar to that of methane in Figure 5A. Here, the conversion of the non-promoted catalyst started at 81.5% and maintained a relatively stable trend with less reduction in time on stream. After 7.5 h, the conversion was about 80%. When the catalyst was promoted with Ce, the CO<sub>2</sub> conversion was enhanced from 9% to 16%. The highest conversion was recorded using the 3% Ce loading catalyst. Loading higher than 3% such as 5% affected negatively affected the conversion due to similar reasons as those shown in Figure 5A. Table 4 summarized the performance comparison between the current work and the work of other investigators. The present catalysts offered superb methane activity.

**Table 4.** Comparison between the CH<sub>4</sub> conversion acquired and those in the literature using different catalysts for the dry reforming of CH<sub>4</sub>.

Catalyst	CH <sub>4</sub> :CO <sub>2</sub>	GHSV <sup>1</sup> (mL/g/h)	T (°C)	% CH <sub>4</sub>	References
10%Ni/8%PO <sub>4</sub> +ZrO <sub>2</sub>	1:1	13000	800	80	[4]
Ni-Zr/SBA-15	1:1	15000	800	88	[30]
Ni-HTNT	1:1	12000	700	74	[45]
0.5% Co/ Ni/γ-Al <sub>2</sub> O <sub>3</sub>	1:1	12000	650	70	[46]
1Co-1Ce-1Ca/AC-N	1:1	720	800	68	[47]
Ni-Ce/Mg-Al-O	1:1	72000	800	86	[48]
10Ni15La/illite-clay	5:4	60000	800	80	[49]
Ni/50% CeO <sub>2</sub> -50% TiO <sub>2</sub>	1:1	14400	750	90	[50]
10%Ni+3%Ce/8%PO <sub>4</sub> +ZrO <sub>2</sub>	1:1	28000	800	95	Present work

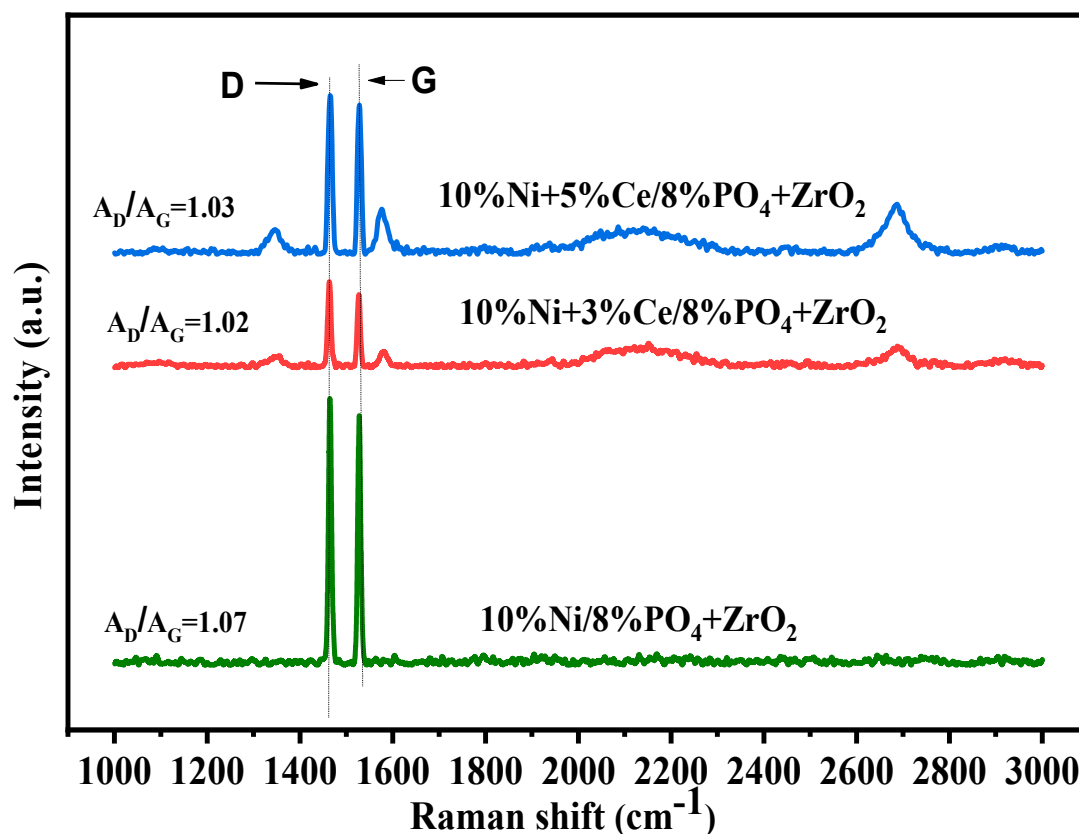
<sup>1</sup> GHSV- Gas Hourly Space Velocity.

Figure 6 exhibits the results obtained from the thermogravimetric (TGA) analysis of spent catalysts. The effect of the different loadings of the cerium promoter was seen in the weight loss. In the early period of the TGA, some catalysts showed a weight increase due to the formation of oxides in the ambient air. A sharp weight loss was observed for all promoted catalysts at 600 °C, ending at about 800 °C. It was observed that the weight loss reduced with the increase in the percentage loading of ceria: from 3% weight loss for the unpromoted catalyst down to about 1% weight loss for the 3%Ce promoted catalyst. There was an increase in the carbon deposits for the catalyst with ceria loading above 3%. It was observed that under this condition, the Ce promoter enhanced the gasification of the carbon deposits, and the percentage loading of 3% appeared to be the optimum.



**Figure 6.** Thermogravimetric (TGA) results of the spent catalysts with 700, 600, and 800 °C activation, calcination, and reaction temperatures, respectively.

Raman spectroscopy was done to study the degree of graphitization characteristics of the formed carbon on the used catalysts. Figure 7 displays the Raman spectra of used catalysts, and it could be noted that all catalysts exhibited two peaks with high intensities in the range between 1400 and 1600  $\text{cm}^{-1}$ . These peaks can be ascribed to the characteristic D and G bands, respectively [51]. The D band is attributed to the imperfections and disorders of the faulty structural carbons, and the G band is related to the vibrations of perfect graphite carbon. The peak areas ratio of the D and G ( $A_D/A_G$ ) bands is used to assess the graphitic degree and the extent of defects in the carbon deposits over the used catalysts; a lower  $A_D/A_G$  ratio designates a well-ordered structure of the carbon deposits found on the used catalysts. There was an increase in the intensity of the peaks for 10 Ni + 5% Ce/8% PO<sub>4</sub> + ZrO<sub>2</sub> relative to that of the 10 Ni + 3% Ce/8% PO<sub>4</sub> + ZrO<sub>2</sub>, indicating more carbon deposits as revealed by the TGA results. The ratio of  $A_D/A_G$  was computed, and this showed that the 10 Ni/8% PO<sub>4</sub> + ZrO<sub>2</sub> (1.07) had the highest value relative to the ceria-promoted samples. This implies that the addition of cerium oxide slightly raised the extent of graphitization of the carbon deposits.



**Figure 7.** Raman spectra of used catalysts of 10 Ni + x% Ce/8% PO<sub>4</sub> + ZrO<sub>2</sub> (x = 0, 3, and 5) catalyst calcined at 600 °C, operated at 800 °C, GHSV = 28,000 (mL/g/h).

### 3. Materials and Methods

#### 3.1. Preparation of Catalyst

The method of wet impregnation was employed for the preparation of catalysts used for the dry reforming of methane. The used procedure was described in our previous paper [4]. The phosphate zirconium was gifted by Daiichi Kigenso Kagaku Kogyo Co., Ltd., Osaka, Japan. The surface area of the support is 246 m<sup>2</sup>/g, while the particle size is 4.73 μm. The compositions of the catalysts and the textural properties such as pore volume (PV), surface area (BET), and pore diameter (PD) are shown in Table 1. Energy dispersive x-ray (EDX) analysis of two catalysts, 10%Ni + 1.5%Ce/8%PO<sub>4</sub> + ZrO<sub>2</sub> and 10%Ni + 1.5%Ce/8%PO<sub>4</sub> + ZrO<sub>2</sub>, was performed. The composition of the total active metals prepared were 11.50% and 13.00%, respectively, while the EDX analysis gave compositions of the total active metals as 11.17 % and 12.96%, indicating close values.

#### 3.2. Catalyst Performance Evaluation

The procedures for CO<sub>2</sub> reforming of methane experiments were performed in a stainless steel tubular reactor (0.91 cm diameter and 0.30 m long). The reactor was obtained from PID Eng. & Tech Microactivity Reference Company. The particle size of the 10 Ni + x% Ce/8% PO<sub>4</sub> + ZrO<sub>2</sub> ((x = 0–5) catalysts ranged between 19.0 and 19.6 nm. The operating pressure of 1 atm was applied during the reforming reactions. An amount of 150 mg of the catalyst was reduced with H<sub>2</sub> flows of 20 mL/min for 30 min at 700 °C. Then, the system was treated with N<sub>2</sub> for 15 min to desorb the physisorbed H<sub>2</sub> from the bed. After that, the reactor temperature was adjusted to 800 °C by the flow of N<sub>2</sub>. In the usual test, the ratio of N<sub>2</sub>/CO<sub>2</sub>/CH<sub>4</sub> was fixed to 2/6/6 at a total flow rate of 70 mL/min, giving a gas hourly space velocity of 28,000 mL (h·gcat)<sup>-1</sup>. The analysis of the catalyst compositions was carried out using a gas chromatograph, which was fitted with a conductivity detector (GC-2014 SHIMADZU, Kyoto,

Japan). After the reaction, the reactor system was flushed with N<sub>2</sub> gas to room temperature. Then, the catalysts were taken for characterization. Afterward, experimental reproducibility was performed by considering an average of triplicate experimental runs. The conversion formula is illustrated below:

$$\%CH_4 \text{ conversion} = \frac{CH_4 \text{ in} - CH_4 \text{ out}}{CH_4 \text{ in}} \times 100 \quad (1)$$

$$\%CO_2 \text{ conversion} = \frac{CO_2 \text{ in} - CO_2 \text{ out}}{CO_2 \text{ in}} \times 100. \quad (2)$$

### 3.3. Catalyst Characterization

#### 3.3.1. N<sub>2</sub> Physisorption

In this work, the textural characteristics of the catalysts were studied by N<sub>2</sub> adsorption–desorption isotherms, which were computed at −197 °C with a Micromeritics Tristar II 3020 porosity and surface area analyzer. In each test, 0.2–0.3 g of catalyst was taken. The samples were previously degassed at 300 °C for 3 h to expel from the catalyst surface undesired adsorbed gases, organics, and water vapor. The BET technique was applied to obtain the surface areas by means of the N<sub>2</sub> adsorption scale in the interval of 0.06–0.35 times the equilibrium pressure.

#### 3.3.2. TPR

The reduction behavior of the catalysts was examined via an AutoChem-II Micromeritics device. The method used to analyze was described in our paper [5].

#### 3.3.3. XRD

To investigate the diffraction profiles of the samples, X-ray diffraction (XRD) measurements of fresh catalysts were used. The XRD was accomplished using Rigaku (Miniflex), with K $\alpha$ -Cu radiation at 40 kV and 40 mA. A 2 $\theta$  range of 10–85° and a scanning step of 0.02° were used.

#### 3.3.4. TGA

The quantification of the total deposited C on the spent catalysts was made employing thermogravimetric analysis (TGA) in air. The unit is a Shimadzu TGA analyzer. From the used catalysts, 10–15 mg was heated at the rate of 20 °C/min from 25 °C to 1000 °C, and the mass loss was registered.

#### 3.3.5. CO<sub>2</sub>-TPD

The Micromeritics Autochem II apparatus, Micromeritics analyzer was used to perform the CO<sub>2</sub>-TPD. A helium gas stream of 30 mL/min was used to outgas 0.05 g of catalyst at 600 °C for 60 min. Then, the catalyst was brought to 50 °C. After that, a CO<sub>2</sub> stream was admitted for 1 h, and the catalyst was then flushed with helium to remove the physically attached CO<sub>2</sub>. The desorption peak profile was registered, while the temperature was varied at 10 °C/min. The CO<sub>2</sub> composition in the output stream was determined using a thermal conductivity detector. The peak areas gave the quantity of CO<sub>2</sub> desorbed.

#### 3.3.6. Raman Spectroscopy

Raman spectra were performed using an NMR-4500 Laser Raman Spectrometer. The excitation beam was adjusted to a wavelength of 532 nm. The measurement was carried out by the objective lens with 20 $\times$  magnification. A 6 mW beam power and an exposure time of 3 min were used. The Raman shift of the spectra was measured in the range of 1000–3000 cm<sup>−1</sup> while Spectra Manager Ver.2 software processed the profiles.

#### 4. Conclusions

Various cerium loadings were used to promote 10% Ni/8% PO<sub>4</sub>+ZrO<sub>2</sub> catalysts. The cerium loadings constituted the values (1%, 1.5%, 2%, 2.5%, 3%, and 5%). These catalysts were used for CO<sub>2</sub> reforming of methane in a fixed bed reactor. The Ce promoter improved the catalytic performance. The highest conversions of CH<sub>4</sub> and CO<sub>2</sub> at 800 °C reaction were obtained using 3% Ce loading. The study of the Raman spectroscopy denoted that the 3% Ce-promoted catalyst possessed the least values of D and G bands, indicating the highest structural perfection. Table 1 also displayed that the 3% Ce loading possesses the highest surface area, the largest pore volume, and the greatest pore diameter. The study of the CO<sub>2</sub>-TPD revealed the enhancement of basicity by the addition of the Ce promoter. Tables 2 and 3 exhibited the highest percentage reduction degree and the highest total basicity were given by the 3% Ce loading catalyst, respectively.

The investigation of the TGA indicated insignificant amounts of carbon deposition and therefore did not pose stimulating effects of carbon deposition onto the surface of the catalyst. The promoted catalysts without exception enhanced the conversions of CH<sub>4</sub> and CO<sub>2</sub>. Among the promoted catalysts tested, The 10Ni + 3%Ce/8%PO<sub>4</sub> + ZrO<sub>2</sub> catalyst system operated at 1 bar and at 800 °C gave the highest conversions of CH<sub>4</sub> (95%) and CO<sub>2</sub> (96%). Thus, steady stability profiles of CH<sub>4</sub> and CO<sub>2</sub> conversions during time on stream for all promoted catalysts were observed.

**Author Contributions:** Experiment and Writing—original draft preparation A.A.I., A.S.A.-F., and S.O.K.; XRD analysis N.S.K., Writing—review and editing, A.E.A. and A.H.F. All authors have read and agreed to the published version of the manuscript.

**Funding:** The work is supported by the Deanship of Scientific Research programs of King Saud University via (project (No. RG-1435-078).

**Acknowledgments:** The KSU authors would like to extend their sincere appreciation to the Deanship of Scientific Research at the King Saud University for its funding for this research group project # (RG-1435-078).

**Conflicts of Interest:** The authors affirm no conflict of interest.

#### References

1. Arora, S.; Prasad, R. An overview on dry reforming of methane: Strategies to reduce carbonaceous deactivation of catalysts. *RSC Adv.* **2016**, *6*, 108668–108688. [CrossRef]
2. Zoundi, Z. CO<sub>2</sub> emissions, renewable energy and the Environmental Kuznets Curve, a panel cointegration approach. *Renew. Sustain. Energy Rev.* **2017**, *72*, 1067–1075. [CrossRef]
3. Hoehne, C.G.; Chester, M.V. Greenhouse gas and air quality effects of auto first-last mile use with transit. *Transp. Res. Part D Transp. Environ.* **2017**, *53*, 306–320.
4. Al-Fatesh, A.S.; Arafat, Y.; Ibrahim, A.A.; Kasim, S.O.; Alharthi, A.; Fakeeha, A.H.; Abasaeed, A.E.; Giuseppe Bonura, G.; Francesco Frusteri, F. Catalytic Behaviour of Ce-Doped Ni Systems Supported on Stabilized Zirconia under Dry Reforming Conditions. *Catalysts* **2019**, *9*, 473. [CrossRef]
5. Al-Fatesh, A.S.; Kasim, S.O.; Ibrahim, A.A.; Fakeeha, A.H.; Abasaeed, A.E.; Alrasheed, R.; Ashamari, R.; Bagabas, A. Combined Magnesia, Ceria and Nickel catalyst supported over  $\gamma$ -Alumina Doped with Titania for Dry Reforming of Methane. *Catalysts* **2019**, *9*, 188. [CrossRef]
6. Lau, C.; Tsolakis, A.; Wyszynski, M. Biogas upgrade to syn-gas (H<sub>2</sub>-CO) via dry and oxidative reforming. *Int. J. Hydrogen Energy* **2011**, *36*, 397–404. [CrossRef]
7. Kwon, B.W.; Oh, J.H.; Kim, G.S.; Yoon, S.P.; Han, J.; Nam, S.W.; Ham, H.C. The novel perovskite-type Ni-doped Sr<sub>0.92</sub>Y<sub>0.08</sub>TiO<sub>3</sub> as a reforming biogas (CH<sub>4</sub> + CO<sub>2</sub>) for H<sub>2</sub> production. *Appl. Energy* **2018**, *227*, 213–219.
8. IEA. *World Energy Outlook 2015*; OECD Publishing: Paris, France, 2015; Available online: <https://doi.org/10.1787/weo-2015-en> (accessed on 10 November 2015).
9. Jiao, F.; Pan, X.; Xiao, J.; Li, H.; Ma, H.; Wei, M.; Pan, Y.; Zhou, Z.; Li, M.; Miao, S.; et al. Selective conversion of syngas to light olefins. *Science* **2016**, *351*, 1065–1068. [CrossRef]
10. Cui, G.; Liu, J.; Wei, M.; Feng, X.; Elsworth, D. Evolution of permeability during the process of shale gas extraction. *J. Nat. Gas Sci. Eng.* **2018**, *49*, 94–109. [CrossRef]

11. Quéllar-Franca, R.M.; Azapagic, A. Carbon capture, storage and utilization technologies: A critical analysis and comparison of their life cycle environmental impacts. *J. CO<sub>2</sub> Util.* **2015**, *9*, 82–102. [[CrossRef](#)]
12. Vieira, M.O.; Aquino, A.S.; Schütz, M.K.; Vecchia, F.D.; Ligabue, R.; Seferin, M.; Einloft, S. Chemical Conversion of CO<sub>2</sub>: Evaluation of Different Ionic Liquids as Catalysts in Dimethyl Carbonate Synthesis. *Energy Procedia* **2017**, *114*, 7141–7149. [[CrossRef](#)]
13. Sheu, E.J.; Mokheimer, E.M.; Ghoniem, A.F. A review of solar methane reforming systems. *Int. J. Hydrogen Energy* **2015**, *40*, 12929–12955. [[CrossRef](#)]
14. García-Diéguez, M.; Finocchio, E.; Larrubia, M. Ángeles; Alemany, L.J.; Busca, G. Characterization of alumina-supported Pt, Ni and PtNi alloy catalysts for the dry reforming of methane. *J. Catal.* **2010**, *274*, 11–20. [[CrossRef](#)]
15. Nawfal, M.; Gennequin, C.; Labaki, M.; Nsouli, B.; Aboukais, A.; AbiAad, E. Hydrogen production by methane steam reforming over Ru supported on NiMgAl mixed oxides prepared via hydrotalcite route. *Int. J. Hydrogen Energy* **2015**, *40*, 1269–1277. [[CrossRef](#)]
16. Al-Fatesh, A.; Singh, S.K.; Kanade, G.; Atia, H.; Fakeeha, A.H.; Ibrahim, A.A.; El-Toni, A.M.; Labhasetwar, N.K. Rh promoted and ZrO<sub>2</sub>/Al<sub>2</sub>O<sub>3</sub> supported Ni/Co based catalysts: High activity for CO<sub>2</sub> reforming, steam–CO<sub>2</sub> reforming and oxy–CO<sub>2</sub> reforming of CH<sub>4</sub>. *Int. J. Hydrogen Energy* **2018**, *43*, 12069–12080. [[CrossRef](#)]
17. Arandiyán, H.; Peng, Y.; Liu, C.; Chang, H.; Li, J. Effects of noble metals doped on mesoporous LaAlNi mixed oxide catalyst and identification of carbon deposit for reforming CH<sub>4</sub> with CO<sub>2</sub>. *J. Chem. Tech. Biotechnol.* **2014**, *89*, 372–381. [[CrossRef](#)]
18. El Hassan, N.; Kaydouh, M.; Geagea, H.; El Zein, H.; Jabbour, K.; Casale, S.; El Zakhem, H.; Massiani, P. Low temperature dry reforming of methane on rhodium and cobalt based catalysts: Active phase stabilization by confinement in mesoporous SBA-15. *Appl. Catal. A Gen.* **2016**, *520*, 114–121. [[CrossRef](#)]
19. Hou, Z.; Chen, P.; Fang, H.; Zheng, X.; Yashima, T. Production of synthesis gas via methane reforming with CO<sub>2</sub> on noble metals and small amount of noble-(Rh)-promoted Ni catalysts. *Int. J. Hydrogen Energy* **2006**, *31*, 555–561. [[CrossRef](#)]
20. Usman, M.; Daud, W.M.A.W.; Abbas, H.F. Dry reforming of methane: Influence of process parameters—A review. *Renew. Sust. Energ. Rev.* **2015**, *45*, 710–744.
21. Akri, M.; Shu Zhao, S.; Xiaoyu Li, X.; Zang, K.; Lee, A.F.; Isaacs, M.A.; Xi, W.; Gangarajula, Y.; Luo, J.; Ren, Y.; et al. Atomically dispersed nickel as coke-resistant active sites for methane dry reforming. *Nat. Commun.* **2019**, *10*, 5181. [[CrossRef](#)]
22. Goula, M.; Charisiou, N.; Siakavelas, G.; Tzounis, L.; Tsiaoussis, I.; Panagiotopoulou, P.; Goula, G.; Yentekakis, I.V. Syngas production via the biogas dry reforming reaction over Ni supported on zirconia modified with CeO<sub>2</sub> or La<sub>2</sub>O<sub>3</sub> catalysts. *Int. J. Hydrogen Energy* **2017**, *42*, 13724–13740. [[CrossRef](#)]
23. Abba, M.O.; Gonzalez-Delacruz, V.M.; Colón, G.; Sebti, S.; Caballero, A. In situ XAS study of an improved natural phosphate catalyst for hydrogen production by reforming of methane. *Appl. Catal. B Environ.* **2014**, *150*, 459–465. [[CrossRef](#)]
24. Ibrahim, A.A.; Al-Fatesh, A.S.; Khan, W.U.; Kasim, S.O.; Abasaeed, A.E.; Fakeeha, A.H.; Bonura, G.; Frusteri, F. Enhanced coke suppression by using phosphate-zirconia supported nickel catalysts under dry methane reforming conditions. *Int. J. Hydrogen Energy* **2019**, *44*, 27784–27794. [[CrossRef](#)]
25. Rostrupnielsen, J.; Hansen, J. CO<sub>2</sub>-Reforming of Methane over Transition Metals. *J. Catal.* **1993**, *144*, 38–49. [[CrossRef](#)]
26. Abdullah, B.; Ghani, N.A.A.; Vo, D.-V.N. Recent advances in dry reforming of methane over Ni-based catalysts. *J. Clean. Prod.* **2017**, *162*, 170–185. [[CrossRef](#)]
27. Luisetto, I.; Tuti, S.; Romano, C.; Boaro, M.; Di Bartolomeo, E.; Kesavan, J.K.; Kumar, S.S.; Selvakumar, K. Dry reforming of methane over Ni supported on doped CeO<sub>2</sub>: New insight on the role of dopants for CO<sub>2</sub> activation. *J. CO<sub>2</sub> Util.* **2019**, *30*, 63–78. [[CrossRef](#)]
28. Li, M.; Van Veen, A.C. Tuning the catalytic performance of Ni-catalysed dry reforming of methane and carbon deposition via Ni-CeO<sub>2</sub>-x interaction. *Appl. Catal. B Environ.* **2018**, *237*, 641–648. [[CrossRef](#)]
29. Kalai, D.Y.; Stangeland, K.; Tucho, W.M.; Jin, Y.; Yu, Z. Biogas reforming on hydrotalcite-derived Ni-Mg-Al catalysts: The effect of Ni loading and Ce promotion. *J. CO<sub>2</sub> Util.* **2019**, *33*, 189–200. [[CrossRef](#)]

30. Chong, C.C.; Teh, L.P.; Setiabudi, H.D. Syngas production via CO<sub>2</sub> reforming of CH<sub>4</sub> over Ni-based SBA-15: Promotional effect of promoters (Ce, Mg, and Zr). *Mater. Today Energy* **2019**, *12*, 408–417. [[CrossRef](#)]
31. Pietraszek, A.; Koubaissy, B.; Roger, A.-C.; Kiennemann, A. The influence of the support modification over Ni-based catalysts for dry reforming of methane reaction. *Catal. Today* **2011**, *176*, 267–271. [[CrossRef](#)]
32. Chein, R.-Y.; Fung, W.-Y. Syngas production via dry reforming of methane over CeO<sub>2</sub> modified Ni/Al<sub>2</sub>O<sub>3</sub> catalysts. *Int. J. Hydrogen Energy* **2019**, *44*, 14303–14315. [[CrossRef](#)]
33. Lino, A.V.P.; Calderon, Y.N.C.; Mastelaro, V.R.; Assaf, E.M.; Assaf, J.M.; Colmenares, Y.N. Syngas for Fischer-Tropsch synthesis by methane tri-reforming using nickel supported on MgAl<sub>2</sub>O<sub>4</sub> promoted with Zr, Ce and Ce-Zr. *Appl. Surf. Sci.* **2019**, *481*, 747–760. [[CrossRef](#)]
34. Li, J.; Chen, J.; Song, W.; Liu, J.; Shen, W. Influence of zirconia crystal phase on the catalytic performance of Au/ZrO<sub>2</sub> catalysts for low-temperature water gas shift reaction. *Appl. Catal. A Gen.* **2008**, *334*, 321–329. [[CrossRef](#)]
35. Li, H.; Wang, J. Study on CO<sub>2</sub> reforming of methane to syngas over Al<sub>2</sub>O<sub>3</sub>–ZrO<sub>2</sub> supported Ni catalysts prepared via a direct sol–gel process. *Chem. Eng. Sci.* **2004**, *59*, 4861–4867. [[CrossRef](#)]
36. Li, Q.; Wu, G.; Cullen, D.A.; More, K.L.; Mack, N.H.; Chung, H.T.; Zelenay, P. Phosphate-Tolerant Oxygen Reduction Catalysts. *ACS Catal.* **2014**, *4*, 3193–3200. [[CrossRef](#)]
37. Hu, L.; Urakawa, A. Continuous CO<sub>2</sub> capture and reduction in one process: CO<sub>2</sub> methanation over unpromoted and promoted Ni/ZrO<sub>2</sub>. *J. CO<sub>2</sub> Util.* **2018**, *25*, 323–329. [[CrossRef](#)]
38. Pan, Q.; Peng, J.; Sun, T.; Wang, S.; Wang, S. Insight into the reaction route of CO<sub>2</sub> methanation: Promotion effect of medium basic sites. *Catal. Commun.* **2014**, *45*, 74–78. [[CrossRef](#)]
39. Salker, A.V.; Naik, S.J. Mechanistic study of acidic and basic sites for CO oxidation over nano based Co<sub>2</sub>xFe<sub>x</sub>WO<sub>6</sub> catalysts. *Appl. Catal. B Environ.* **2009**, *89*, 246–254. [[CrossRef](#)]
40. Singh, H.; Rai, A.; Yadav, R.; Sinha, A.K. Glucose hydrogenation to sorbitol over unsupported mesoporous Ni/NiO catalyst. *Mol. Catal.* **2018**, *451*, 186–191.
41. Wang, C.; Sun, N.; Zhao, N.; Wei, W.; Zhao, Y. Template-free preparation of bimetallic mesoporous Ni-Co-CaO-ZrO<sub>2</sub> catalysts and their synergetic effect in dry reforming of methane. *Catal. Today* **2017**, *281*, 268–275. [[CrossRef](#)]
42. Alipour, Z.; Rezaei, M.; Meshkani, F. Effect of Ni loadings on the activity and coke formation of MgO-modified Ni/Al<sub>2</sub>O<sub>3</sub> nanocatalyst in dry reforming of methane. *J. Energy Chem.* **2014**, *23*, 633–638. [[CrossRef](#)]
43. Ding, M.; Tu, J.; Zhang, Q.; Wang, M.; Tsubaki, N.; Wang, T.; Ma, L. Enhancement of methanation of bio-syngas over CeO<sub>2</sub>-modified Ni/Al<sub>2</sub>O<sub>3</sub> catalysts. *Biomass-Bioenergy* **2016**, *85*, 12–17. [[CrossRef](#)]
44. Conner, W.C.; Falconer, J.L. Spillover in Heterogeneous Catalysis. *Chem. Rev.* **1995**, *95*, 759–788. [[CrossRef](#)]
45. Monteiro, W.F.; Vieira, M.O.; Calgaro, C.O.; Perez-Lopez, O.W.; Ligabue, R.A. Dry reforming of methane using modified sodium and protonated titanate nanotube catalysts. *Fuel* **2019**, *253*, 713–721. [[CrossRef](#)]
46. Cao, K.; Gong, M.; Yang, J.; Cai, J.; Chu, S.; Chen, Z.; Shan, B.; Chen, R. Nickel catalyst with atomically-thin meshed cobalt coating for improved durability in dry reforming of methane. *J. Catal.* **2019**, *373*, 351–360. [[CrossRef](#)]
47. Sun, Y.; Zhang, G.; Xu, Y.; Zhang, R. Dry reforming of methane over Co-Ce-M/AC-N catalyst: Effect of promoters (Ca and Mg) and preparation method on catalytic activity and stability. *Int. J. Hydrogen Energy* **2019**, *44*, 22972–22982. [[CrossRef](#)]
48. Fang, X.; Zhang, J.; Liu, J.; Wang, C.; Huang, Q.; Xu, X.; Peng, H.; Liu, W.; Wang, X.; Zhou, W. Methane dry reforming over Ni/Mg-Al-O: On the significant promotional effects of rare earth Ce and Nd metal oxides. *J. CO<sub>2</sub> Util.* **2018**, *25*, 242–253. [[CrossRef](#)]
49. Akri, M.; Pronier, S.; Chafik, T.; Achak, O.; Granger, P.; Simon, P.; Trentesaux, M.; Batiot-Dupeyrat, C. Development of nickel supported La and Ce-natural illite clay for autothermal dry reforming of methane: Toward a better resistance to deactivation. *Appl. Catal. B Environ.* **2017**, *205*, 519–531. [[CrossRef](#)]

50. Kim, S.S.; Lee, S.M.; Won, J.M.; Yang, H.J.; Hong, S.C. Effect of Ce/Ti ratio on the catalytic activity and stability of Ni/CeO<sub>2</sub>-TiO<sub>2</sub> catalyst for dry reforming of methane. *Chem. Eng. J.* **2015**, *280*, 433–440. [[CrossRef](#)]
51. Chen, X.; Oh, W.-D.; Hu, Z.-T.; Sun, Y.-M.; Webster, R.D.; Li, S.-Z.; Lim, T.-T. Enhancing sulfacetamide degradation by peroxymonosulfate activation with N-doped graphene produced through delicately-controlled nitrogen functionalization via tweaking thermal annealing processes. *Appl. Catal. B Environ.* **2018**, *225*, 243–257. [[CrossRef](#)]



© 2020 by the authors. Licensee MDPI, Basel, Switzerland. This article is an open access article distributed under the terms and conditions of the Creative Commons Attribution (CC BY) license (<http://creativecommons.org/licenses/by/4.0/>).